Electronic Supplementary Material (ESI) for Nanoscale

Electronic Supplementary Information for

Metalation of tetraphenylporphyrin with nickel on a TiO$_2$(110)-1×2 surface

Cici Wang,[a] Qitang Fan,[a] Yong Han,[a] José I. Martínez,[b] José A. Martín-Gago,[b] Weijia Wang,[a] Huanxin Ju,[a] J. Michael Gottfried [*c] and Junfa Zhu[*a]

[a]National Synchrotron Radiation Laboratory and Collaborative Innovation Center of Suzhou Nano Science and Technology, University of Science and Technology of China, Hefei, 230029, P. R. China, jfzhu@ustc.edu.cn.
[b]ESISNA Group, Dept. Surfaces, Coatings and Molecular Astrophysics, Institute of Material Science of Madrid (ICMM-CSIC), Sor Juana Inés de la Cruz, 3, 28049, Madrid , Spain.
[c]Fachbereich Chemie, Philipps-Universität Marburg, Hans-Meerwein-Str. 4, 35032, Marburg, Germany, michael.gottfried@chemie.uni-marburg.de.

THEORETICAL METHODOLOGY

Computational Details

For the *ab initio* structural optimization, molecular dynamics, electronic structure, transition-state barriers and theoretical STM-imaging simulations of the different adsorbate / TiO$_2$(110) configurations analysed in this paper, Density Functional Theory (DFT) was used effectively combining the localized-basis-set and plane-wave schemes as implemented in the FIREBALL[1] and QUANTUM ESPRESSO[2] simulation packages, respectively. A perturbative van der Waals (vdW) correction was used to check the reliability of all the adsorbed adlayer configurations. For this purpose, we have used an empirical efficient vdW R^{-6} correction to add dispersive forces to conventional density functional (DFT+D)[3]. Within this approach, the vdW correction is added to the DFT total energy by the expression:

$$E_{vdW} = \sum_{i,j} \frac{C_{ij}}{R_{ij}^6} f(R_{ij}),$$

(eq. [1])

where C_{ij} and R_{ij} are the vdW coefficients and the distance between atom i and j, respectively. The vdW coefficients can be calculated as described by Elstner *et al.*[4] In eq. [1], $f(R_{ij})$ is a damping function that prevents a divergence in the energy as R_{ij} tends to zero as:

$$f(R_{ij}) = \left(1 - exp\left[-3.0\left(\frac{R_{ij}}{R_{0ij}}\right)^7\right]\right)^4,$$

(eq. [2])

where R_{0ij} is the sum of atomic van der Waals radii. They can be calculated from the vdW radii provided by Gavezzotti and co-workers (see further details on this approach in Refs. 3, 4 and references therein).

The localized-basis-set code FIREBALL is based on a local-orbital formulation of DFT in which self-

consistency is implemented on the orbital occupation numbers;[5, 6] these orbital occupation numbers have been obtained using the orthonormal Löwdin orbitals.[1,6-8] We have used a basis set of optimized *spd* numerical atomic orbitals (NAOs)[9] for C, N, Ni and Ti, ss*pp* for O and s for H, For the plane-wave code QUANTUM ESPRESSO, one-electron wave-functions were expanded in a basis of plane-waves, with energy cut-offs of 400 and 500 eV for the kinetic energy and for the electronic density, respectively, which have been adjusted to achieve sufficient accuracy in the total energy. The exchange-correlation (XC) effects have been accounted by using the local density PW91 parametrization[10] and norm-conserving scalar-relativistic pseudopotentials[11] have been considered to model the ion-electron interaction. In the calculations, the Brillouin zones (BZ) were sampled by means of optimal Monkhorst-Pack grids[12] guaranteeing a full convergence in energy and electronic density.

Transition State Barriers

Transition states (TSs) have been investigated here within the climbing-image nudge elastic band (CI-NEB) approach[13-15] implemented in the QUANTUM ESPRESSO package[2], where the initial, the final, and a sufficient amount of intermediate image-states were free to fully relax. This CI-NEB method has several desirable advantages, including: i) it converges to a Minimum Energy Path (MEP), providing sufficient resolution in the discrete representation of the path, when enough images are included in the chain, ii) it only requires evaluation of the interaction energy and the first derivative of the energy with respect to coordinates, iii) the convergence to the MEP is decoupled from the discrete representation of the path, making the former robust and the latter flexible, and, finally, iv) the method is guaranteed to give a continuous path even when multiple MEPs exist.

Theoretical STM imaging

To conclude the theoretical framework description, once the electronic structure has been adequately established, theoretical STM calculations have been performed for all the interfacial configurations considered in this study, to be compared with the experimental evidence. In order to obtain accurate STM images and tunnelling currents, we used an efficient STM theoretical simulation technique implemented in the FIREBALL code[1] that includes a detailed description of the electronic properties of both the tip and the sample. Using this technique, based on a combination of a Keldysh Green's function formalism and local orbital density functional theory (DFT),[16, 17] we split the system into sample and tip, where the samples here are the different systems tested. In these calculations we have assumed to simulate the scanning with a W-tip formed by 5 atoms (one of them in the apex) attached to an extended W(100)-crystal. Within this approach, in the tunnelling regime at low temperature, the STM current is given by: [16, 17]

$$I = \frac{4\pi e^2}{\hbar} \int\limits_{E_F}^{E_F + eV_s} d\omega Tr\big[T_{ts}\rho_{ss}(\omega)T_{st}\rho_{tt}(\omega - eV)\big]$$

(eq. 3)

where V_s is the surface voltage, $\boldsymbol{\rho}_{tt}$ and $\boldsymbol{\rho}_{ss}$ are the density of states (DOS) matrices – in the local orbital basis – associated with the tip and sample, whilst $\boldsymbol{T}_{ts}$ and $\boldsymbol{T}_{st}$ are the local orbital Hamiltonian matrices coupling tip and sample. The overlapping Hamiltonian is obtained by using a dimer approximation: a dimer formed by one W atom (corresponding to the tip) and another (H, C, N, O, Ti and Ni coming from the sample) is calculated for different atom–atom distances and for all the non-zero interactions, using the Keldish-Green formalism to propagate the tunnel current between both subsystems. All the theoretical STM images have been obtained at constant-current scanning conditions, moving the W-tip

perpendicularly to the sample in each scanning stage to search a pre-selected fix value of the tunnel current in order to mimic experimental procedure.

Models

The $TiO_2(110)$-1×1, the $TiO_2(110)$-1×2 and the cross-linked (CL) $TiO_2(110)$-1×2 surfaces were modeled in a repeated slab geometry with: (i) a slab of four physical $TiO_2(110)$ layers with a distance >25 Å of vacuum between neighboring cells along the axis perpendicular to the surface; as well as (ii) full periodic boundary conditions representing infinite $TiO_2(110)$ surfaces. In all cases, a perfectly TiO_2 balanced stoichiometry was used in order to avoid surface polarization effects, being the obtained size for the unit cells in the direction parallel to the surface, after full lattice optimization: (18.0×19.8) Å^2 for the case of 2HTPP on the $TiO_2(110)$-1×1 surface, (23.8×21.6) Å^2 for the case of NiTPP on the $TiO_2(110)$-1×1 surface, and (26.5×24.0) Å^2 for all the cases involving the $TiO_2(110)$-1×2 and the cross-linked $TiO_2(110)$-1×2 surfaces. For the full geometry optimizations only the two bottom TiO_2 physical layers were kept fixed in the calculations, in such a way that all the non-fixed atoms were free to move up to achieve residual forces lower than 0.01 eV/Å. In the calculations with the 2HTPP and NiTPP adsorbed on the different surfaces the minimum distance between neighboring molecules was sufficient to minimize the intermolecular interaction. Additionally, in order to check the total energy results for the optimized geometrical configurations, ground-state calculations were recalculated by including an additional oxide layer, with no significant variations with respect to the four physical substrate layers case, guaranteeing the energetical convergence in the results for the different configurations (with an estimated uncertainty below 0.01 eV).

It is well-known how the thickness of the slabs mimicking the rutile surfaces and, in particular, of $TiO_2(110)$, plays a crucial role for the accurate establishment of the electronic properties in this kind of surfaces.[18] However, such accurate theoretical analyses of the electronic properties across the slab thickness are not especially significant in this case mainly for two reasons: i) To find trustable optimal adsorption molecular geometries in the characterization of the different organic/oxide interfaces, the control of the electronic properties of inner TiO_2 layers up to such a high level of accuracy is not so important (once one carries out a detailed convergence study of the adsorption energy in a given interface with the number of physical oxide layers), and particularly in this case where the dispersion forces play such an important role in the interaction. The latest statement is adequately justified in recent literature by some of the coauthors of this manuscript.[19-22] ii) The $TiO_2(110)$-1×2 reconstruction will not follow the electronic characterization pattern reported in those references, which just analyse the $TiO_2(110)$-1×1 case. The $TiO_2(110)$-1×2 reconstruction exhibits characteristic surface conducting rows, which make the topmost layer to behave in a very different manner as compared to the wide-gap semiconducting character of the $TiO_2(110)$-1×1 conventional phase.

Experimental Results Analysis

The metalation reaction between tetraphenylporphyrin and nickel atoms on $TiO_2(110)$-1×2 can additionally be proved by valence band spectra as shown in Fig. S1. The main change is the peak located at ~4 eV lose intensity which is similar to that of NiTPP. The increase of the peak intensity near Fermi edge is due to the d orbital of nickel.[23] The metalation reaction follows the equation: Ni(ads) + 2HTPP(ads) → NiTPP(ads) + H$_2$(g). According to the previous study, the pyrrolic hydrogen atoms are transferred to the metal atom to form weakly bound H$_2$, which desorbs from the surface immediately.[24]
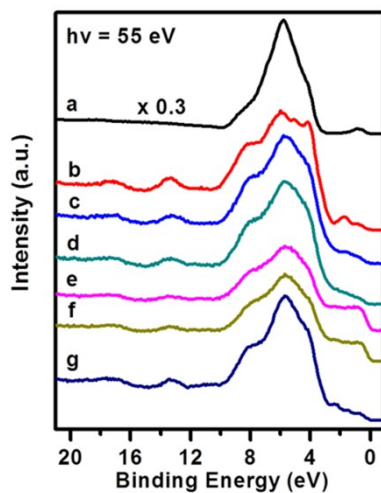
Fig. S1 Valence band spectra of (a) the clean $TiO_2(110)$-1×2 surface, (b) with a monolayer of 2HTPP, (θ_{2HTPP} = 0.197), (c-e) after incremental deposition of Ni onto the sample with Ni/2HTPP ratios of 1:1, 2:1, 3:1 at 300 K, and (f) after heating sample (e) to 550 K. (g) a monolayer of NiTPP on $TiO_2(110)$-1×2 for comparison. The spectra were measured with a photon energy of 55 eV.
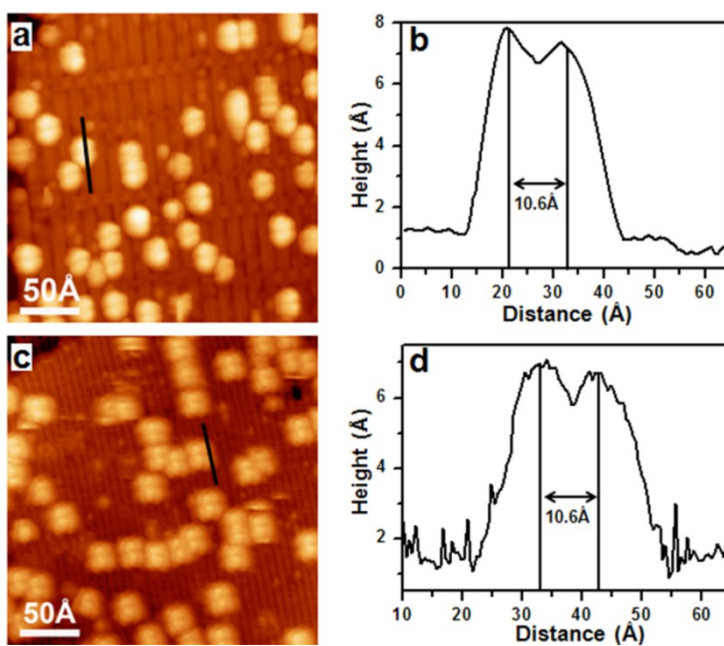

Fig. S2 The STM images of 2HTPP on (a) $TiO_2(110)$-1×2 and (c) $TiO_2(110)$-1×1. (b,d) Apparent height profiles along the black lines shown in (a) and (c), respectively.

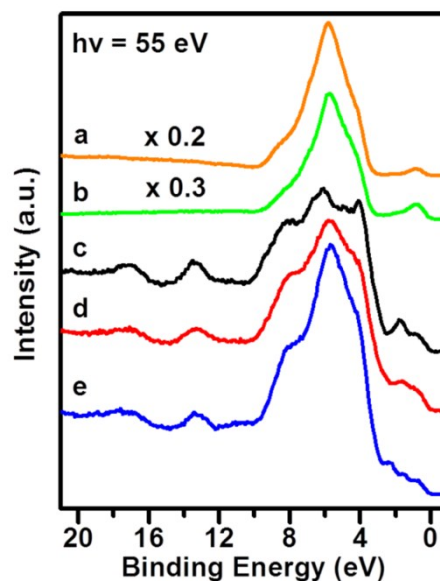Fig. S3 Valence band spectra of (a) the clean $TiO_2(110)$-1×2 surface, (b) pre-deposited Ni on $TiO_2(110)$-1×2 at 300 K, θ_{Ni} = 0. 197. (c) 2HTPP monolayer on pre-deposited Ni on $TiO_2(110)$-1×2 at 300 K, (d) after heating sample (c) to 550 K. (e) a monolayer of NiTPP on $TiO_2(110)$-1×2 for comparison. The photon energy was 55 eV.
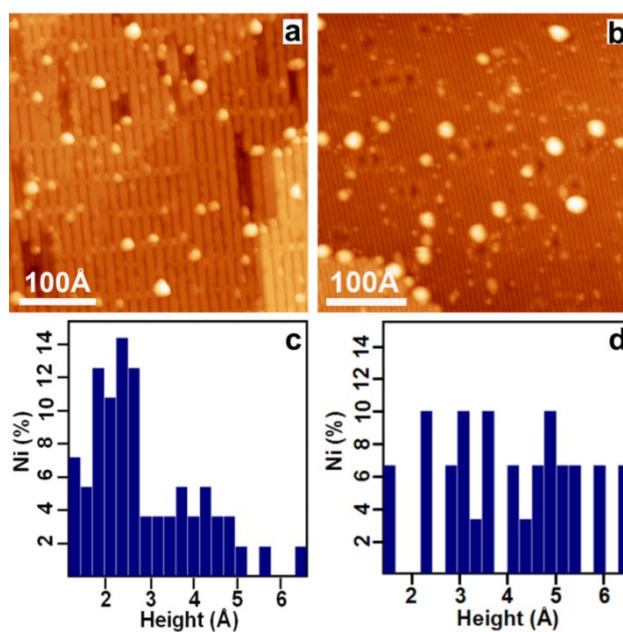

Fig. S4 The STM images of predepositing Ni on (a) $TiO_2(110)$-1×2 and (b) $TiO_2(110)$-1×1 surface. (c,d) Histograms show corresponding Ni cluster heights distributions on the two surfaces.

References

1. J. P. Lewis, P. Jelínek, J. Ortega, A. A. Demkov, D. G. Trabada, B. Haycock, H. Wang, G. Adams, J. K. Tomfohr, E. Abad, H. Wang and D. A. Drabold, *Phys. Stat. Sol. B*, 2011, **248**, 1989-2007.
2. P. Giannozzi, S. Baroni, N. Bonini, M. Calandra, R. Car, C. Cavazzoni, D. Ceresoli, G. L. Chiarotti, M. Cococcioni, I. Dabo, A. Dal Corso, S. de Gironcoli, S. Fabris, G. Fratesi, R. Gebauer, U. Gerstmann, C. Gougoussis, A. Kokalj, M. Lazzeri, L. Martin-Samos, N. Marzari, F. Mauri, R. Mazzarello, S. Paolini, A. Pasquarello, L. Paulatto, C. Sbraccia, S. Scandolo, G. Sclauzero, A. P. Seitsonen, A. Smogunov, P. Umari and R. M. Wentzcovitch, *J. Phys.: Condens. Matter*, 2009, **21**, 395502.
3. S. Grimme, *J. Comp. Chem.*, 2006, **27**, 1787-1799.

4.   V. Barone, M. Casarin, D. Forrer, M. Pavone, M. Sambi and A. Vittadini, *J. Comput. Chem.*, 2009, **30**, 934-939.
5.   A. A. Demkov, J. Ortega, O. F. Sankey and M. P. Grumbach, *Phys. Rev. B*, 1995, **52**, 1618-1630.
6.   F. J. García-Vidal, J. Merino, R. Pérez, R. Rincón, J. Ortega and F. Flores, *Phys. Rev. B*, 1994, **50**, 10537-10547.
7.   J. P. Lewis, K. R. Glaesemann, G. A. Voth, J. Fritsch, A. A. Demkov, J. Ortega and O. F. Sankey, *Phys. Rev. B*, 2001, **64**, 195103.
8.   P. Jelínek, H. Wang, J. P. Lewis, O. F. Sankey and J. Ortega, *Phys. Rev. B*, 2005, **71**, 235101.
9.   M. A. Basanta, Y. J. Dappe, P. Jelínek and J. Ortega, *Comput. Mater. Sci.*, 2007, **39**, 759-766.
10. J. P. Perdew, J. A. Chevary, S. H. Vosko, K. A. Jackson, M. R. Pederson, D. J. Singh and C. Fiolhais, *Phys. Rev. B*, 1992, **46**, 6671-6687.
11. D. Vanderbilt, *Phys. Rev. B*, 1990, **41**, 7892-7895.
12. H. J. Monkhorst, J. D. Pack, *Phys. Rev. B*, 1976, **13**, 5188-5192.
13. B. J. Berne, G. Ciccotti and D. F. Coker, World Scientific Publishing Company: Singapore, 1998.
14. G. Henkelman and H. Jónsson, *J. Chem. Phys.,* 2000, **113**, 9978-9985.
15. G. Henkelman, B. P. Uberuaga and H. Jónsson, *J. Chem. Phys.*, 2000, **113**, 9901-9904.
16. J. M. Blanco, C. González, P. Jelínek, J. Ortega, F. Flores and R. Pérez, *Phys. Rev. B*, 2004, **70**, 085405.
17. J. M. Blanco, F. Flores and R. Pérez, *Prog. Surf. Sci.*, 2006, **81**, 403-443.
18. T. Bredow, L. Giordano, F. Cinquini and G. Pacchioni, *Phys. Rev. B*, 2004, **70**, 035419.
19. J. I. Martínez, F. Flores, J. Ortega, S. Rangan, C. Ruggieri and R. Bartynski, *J. Phys. Chem. C*, 2015, **119**, 22086-22091.
20. G. Otero-Irurueta, J. I. Martínez, G. Lovat, V. Lanzilotto, J. Méndez, M. F. López, L. Floreano, and J. A. Mart ín-Gago, *J. Phys. Chem. C*, 2015, **119**, 7809-7816.
21. C. S. Sánchez, J. I. Martínez, V. Lanzilotto, G. Biddau, B. Gómez-Lor, R. Pérez, L. Floreano, M. F. López and J. A. Martín-Gago, Nanoscale, 2013, **5**, 11058-11065.
22. C. Sánchez-Sánchez, J. I. Martínez, V. Lanzilotto, J. Méndez, J. A. Martín-Gago and M. F. López, *J. Phys. Chem. C*, 2014, **118**, 27318-27324.
23.   G. Di Santo, C. Castellarin-Cudia, M. Fanetti, B. Taleatu, P. Borghetti, L. Sangaletti, L. Floreano, E. Magnano, F. Bondino and A. Goldoni, J. Phys. Chem. C, 2011, **115**, 4155-4162.
24. T. E. Shubina, H. Marbach, K. Flechtner, A. Kretschmann, N. Jux, F. Buchner, H.-P. Steinrück, T. Clark and J. M. Gottfried, J. Am. Chem. Soc., 2007, **129**, 9476-9483.